A CENTRAL-UPWIND GEOMETRY-PRESERVING
METHOD FOR HYPERBOLIC CONSERVATION
LAWS ON THE SPHERE

ABDELAZIZ BELJADID AND PHILIPPE G. LEFLOCH

msp

A CENTRAL-UPWIND GEOMETRY-PRESERVING METHOD FOR HYPERBOLIC CONSERVATION LAWS ON THE SPHERE

ABDELAZIZ BELJADID AND PHILIPPE G. LEFLOCH

We introduce a second-order, central-upwind finite volume method for the discretization of nonlinear hyperbolic conservation laws on the two-dimensional sphere. The semidiscrete version of the proposed method is based on a technique of local propagation speeds, and the method is free of any Riemann solver. The main advantages of our scheme are its high resolution of discontinuous solutions, its low numerical dissipation, and its simplicity of implementation. We do not use any splitting approach, which is often applied to upwind schemes in order to simplify the resolution of Riemann problems. The semidiscrete form of our scheme is strongly built upon the analytical properties of nonlinear conservation laws and the geometry of the sphere. The curved geometry is treated here in an analytical way so that the semidiscrete form of the proposed scheme is consistent with a geometric compatibility property. Furthermore, the time evolution is carried out by using a total-variation diminishing Runge–Kutta method. A rich family of (discontinuous) stationary solutions is available for the conservation laws under consideration when the flux is nonlinear and foliated (in a suitable sense). We present a series of numerical tests, encompassing various nontrivial steady state solutions and therefore providing a good validation of the accuracy and efficiency of the proposed central-upwind finite volume scheme. Our numerical tests confirm that the scheme is stable and succeeds in accurately capturing discontinuous steady state solutions to conservation laws posed on the sphere.

1. Introduction

Nonlinear hyperbolic problems involving conservation laws, or more generally balance laws, arise in continuum physics and in many engineering applications. One of the most important partial differential equations (PDEs) is Burgers' equation, which plays a crucial role in designing numerical methods and arises in a variety of applications. For instance, it arises in the modeling of water infiltration in unsaturated soil and fluid flows through porous media, which are significant in petroleum and environmental engineering problems and in traffic flow problems [11;

37; 31]. In general, the solutions to hyperbolic PDEs can develop sharp gradients (or discontinuities) in finite time, even when starting from smooth initial conditions. For example, in multiphase flow in unsaturated porous media, the wetting front can be very sharp [28; 29]. High-resolution shock-capturing techniques are required since they have the ability to capture sharp gradients within a few computational cells with low levels of numerical diffusion and oscillation.

Various classes of so-called shock-capturing schemes have been proposed. In particular, upwind and central schemes have been used to numerically solve hyperbolic conservation laws. Generally, it can be stated that the difference between these schemes is that upwind methods use characteristic-related information, while central methods do not. The use of characteristic information in upwind schemes can improve the results but renders these schemes, in some cases, computationally expensive. Central schemes are widely used (see, e.g., [32]) after the pioneering work of Nessyahu and Tadmor [34], where a second-order finite volume central method on a staggered grid in spacetime was first proposed. This strategy leads to high resolution and the simplicity of the Riemann-solver free method. As observed by Kurganov and Tadmor [20], this scheme suffers from excessive numerical viscosity when a small time step is considered.

In order to improve the performance of central schemes, some characteristic information can still be used. Kurganov et al. [16] proposed the central-upwind schemes which are based on information obtained from the local speeds of wave propagation. The central-upwind schemes can be considered as a generalization of central schemes originally developed by Kurganov and Tadmor [20; 21] and Kurganov and Levy [14]. The central-upwind schemes are simple, since they use no Riemann solvers, and they have proven their effectiveness in multiple studies, as shown in [18; 19; 15]. Kurganov and Petrova [17] extended the central-upwind schemes to triangular grids for solving two-dimensional Cartesian systems of conservation laws. Next, Beljadid et al. [4] proposed a two-dimensional well-balanced and positivity-preserving cell-vertex central-upwind scheme for the computation of shallow water equations with source terms due to bottom topography.

Several studies have been recently done for hyperbolic conservation laws posed on curved manifolds. The solutions of conservation laws including the systems on manifolds and on spacetimes were studied in [35; 33] and by LeFloch and coauthors [1; 2; 5; 6; 23; 26; 27]. More recently, hyperbolic conservation laws for an evolving surface were investigated by Dziuk, Kröner, and Müller [10], Giesselman [12], and Dziuk and Elliott [9]. Earlier on, for such problems, Ben-Artzi and LeFloch [6] and LeFloch and Okutmustur [27] established a general well-posedness theory for conservation laws on manifolds. In fact, several physically relevant classes of conservation laws in curved spaces were extensively investigated in recent years and we refer the interested reader to [8; 13; 22; 24; 25].

Burgers' equation provides a simple, yet challenging, equation which admits discontinuous solutions, and it provides a simplified setup for the design and validation of shock-capturing numerical methods. Burgers' equation and its generalizations to a curved manifold have been widely used in the physical and mathematical literature. In [3], we have used a class of Burgers-type equations on the sphere and adopted the methodology first proposed by Ben-Artzi, Falcovitz, and LeFloch [5], which uses second-order approximations based on generalized Riemann problems. In [3], a scheme was proposed which uses piecewise linear reconstructions based on solution values at the centers of the computational cells and on values of Riemann solutions at the cell interfaces. A second-order approximation based on a generalized Riemann solver was then proposed, together with a total-variation diminishing Runge–Kutta method (TVDRK3) with operator splitting for the temporal integration.

The finite volume method developed in [5] is strongly linked to the structure of the governing equation on the sphere. The geometric dimensions are considered in an analytical way which leads to discrete forms of schemes that respect exactly the geometric compatibility property. The splitting approach which is used in these schemes simplifies the resolution of the Riemann problem, but it increases the computational cost.

In the present study, we propose a new finite volume method which is less expensive in terms of computational cost. This scheme is free of any Riemann solver and does not use any splitting approach, while such a splitting is widely used in upwind schemes when one needs to simplify the resolution of Riemann problems. The present paper provides the first study of *geometry-preserving, central-upwind schemes for conservation laws on a curved geometry*.

Burgers' equation and its generalizations will be used in the present paper in order to develop and validate the new finite volume method. We design in full detail a geometry-compatible central-upwind scheme for scalar nonlinear hyperbolic conservation laws on the sphere. This system has a simple appearance, but it generates solutions that have a very rich wave structure (due to the curved geometry), and its solutions provide an effective framework for assessing numerical methods. Our goal is to develop and validate a finite volume method which is free of any Riemann problem and is consistent with the geometric compatibility (or divergence-free) condition, at the discrete level. As we prove, the proposed scheme is efficient and accurate for discontinuous solutions and implies only negligible geometric distortions on the solutions.

An outline of the paper is as follows. In Section 2, the governing equations related to this study are presented. Section 3 is devoted to the derivation of the semidiscrete version of our scheme. In Section 4, the coordinate system and the nonoscillatory reconstruction are described. In Section 5, we present the geometry-compatible flux vectors and some particular steady state solutions as well as confined

solutions, which will be used to validate the performance of the proposed method. In Section 6, we demonstrate the high-resolution of the proposed central-upwind scheme thanks to a series of numerical experiments. Finally, some concluding remarks are provided.

2. Governing equations

We consider nonlinear hyperbolic equations posed on the sphere $\mathbb{S}^2$ and based on the flux vector $F = F(x, u)$, depending on the function $u(t, x)$ and the space variable x. This flux is assumed to satisfy the following geometric compatibility condition: for any arbitrary constant value $\bar{u} \in \mathbb{R}$,

$$\nabla \cdot (F(\,\cdot\,, \bar{u})) = 0. \tag{2-1}$$

We also assume that the flux takes the form

$$F(x, u) = n(x) \wedge \Phi(x, u), \tag{2-2}$$

where $n(x)$ is the unit normal vector to the sphere and the function $\Phi(x, u)$ is a vector field in $\mathbb{R}^3$, restricted to $\mathbb{S}^2$ and defined by

$$\Phi(x, u) = \nabla h(x, u). \tag{2-3}$$

Here, $h = h(x, u)$ is a smooth function depending on the space variable x and the state variable $u(t, x)$. Observe that (for instance by Claim 2.2 in [5]) the conditions (2-2) and (2-3) for the flux vector are sufficient to ensure the validity of the geometric compatibility condition (2-1).

Here we are going to develop and validate a new geometry-preserving central-upwind scheme which approximates solutions to the hyperbolic conservation law

$$\partial_t u + \nabla \cdot F(x, u) = 0, \quad (x, t) \in \mathbb{S}^2 \times \mathbb{R}_+, \tag{2-4}$$

where $\nabla \cdot F$ is the divergence of the vector field F. Given any data u_0 prescribed on the sphere, we consider the following initial condition for the unknown function $u = u(t, x)$:

$$u(0, x) = u_0(x), \quad x \in \mathbb{S}^2. \tag{2-5}$$

Equation (2-4) can be rewritten, using general local coordinates and the index of summation j, in the form

$$\partial_t u + \frac{1}{\sqrt{|g|}} \partial_j (\sqrt{|g|} F^j(x, u)) = 0, \tag{2-6}$$

or

$$\partial_t (\sqrt{|g|} u) + \partial_j (\sqrt{|g|} F^j(x, u)) = 0, \tag{2-7}$$

where in local coordinates $x = (x^j)$, the derivatives are denoted by $\partial_j = \frac{\partial}{\partial x^j}$, F^j are the components of the flux vector, and g is the metric.

The conservation law (2-4) becomes

$$\partial_t v + \partial_j(\sqrt{|g|}F^j(x, v/\sqrt{|g|})) = 0, \qquad (2\text{-}8)$$

where $v = u\sqrt{|g|}$. This form will be used in the derivation of the semidiscrete form of the proposed scheme. For the latitude-longitude grid on the sphere, the divergence operator of the flux vector is

$$\nabla \cdot F = \frac{1}{\cos\phi}\left(\frac{\partial}{\partial\phi}(F_\phi\cos\phi) + \frac{\partial F_\lambda}{\partial\lambda}\right), \qquad (2\text{-}9)$$

where F_ϕ and F_λ are the flux components in the latitude (ϕ) and longitude (λ) directions on the sphere, respectively.

3. Derivation of the proposed method

Discretization of the divergence operator. We will describe the derivation of the new central-upwind scheme in detail for the three steps: reconstruction, evolution, and projection. We will develop and give a semidiscrete form of the proposed method for a general computational grid used to discretize the sphere. We assume the discretization of the sphere $\mathbb{S}^2 = \bigcup_{j=1}^{j=N} C_j$, where C_j are the computational cells with areas $|C_j|$. We denote by m_j the number of cell sides of C_j and by $C_{j1}, C_{j2}, \ldots, C_{jm_j}$ the neighboring computational cells that share with C_j the common sides $(\partial C_j)_1, (\partial C_j)_2, \ldots, (\partial C_j)_{m_j}$, respectively. The length of each cell interface $(\partial C_j)_k$ is denoted by l_{jk}. The discrete value of the state variable $u(t, x)$ inside the computational cell C_j at a point $G_j \in C_j$ is denoted by u_j^n at step n. The longitude and latitude coordinates of the suitable point G_j to use inside each computational cell C_j are presented on page 97. These coordinates should be chosen according to the reconstruction of the state variable $u(t, x)$ over the computational cells used on the sphere. Finally, we use the notations Δt and $t_n = n\Delta t$ for the time step and the time at step n, respectively. To obtain the semidiscrete form of the proposed scheme, a first-order explicit development in time will be used. The resulting ODE can be numerically solved using a higher-order SSP ODE solver such as Runge–Kutta of the multistep methods. In the numerical experiments, the third-order TVD Runge–Kutta method proposed by Shu and Osher [36] is used.

In this section, we will present a general form of the discretization of the divergence operator for a general computational grid on the sphere. The approximation of the flux divergence can be written using the divergence theorem as

$$[\nabla \cdot F(x, u)]^{\text{approx}} = \frac{I_j}{|C_j|}, \quad I_j = \left[\oint_{\partial C_j} F(x, u) \cdot \nu(x)\, ds\right]^{\text{approx}}, \qquad (3\text{-}1)$$

where $\nu(x)$ is the unit normal vector to the boundary ∂C_j of the computational cell C_j and ds is the infinitesimal length along ∂C_j.

The scalar potential function h is used to obtain the following approximation along each side of the computational cell C_j.

Claim 3.1. *For a three-dimensional flux $\Phi(x, u)$ given by (2-3), where $h = h(x, u)$ is a smooth function in the neighborhood of the sphere $\mathbb{S}^2$, the total approximate flux through the cell interface e is given by*

$$\oint_{e^1}^{e^2} F(x, u) \cdot v(x) \, ds = -(h(e^2, u_j) - h(e^1, u_j)), \tag{3-2}$$

where e^1 and e^2 are the initial and final endpoints of the side e in the sense of integration and u_j is the estimate value of the variable u along the side e.

Namely, the flux vector is written in the form $F(x, u) = n(x) \wedge \Phi(x, u)$ and we can derive the approximation of the integral along each cell side of C_j

$$\oint_{e^1}^{e^2} F(x, u) \cdot v(x) \, ds = \oint_{e^1}^{e^2} (n(x) \wedge \Phi(x, u)) \cdot v(x) \, ds$$

$$= -\oint_{e^1}^{e^2} \Phi(x, u) \cdot (n(x) \wedge v(x)) \, ds = -\oint_{e^1}^{e^2} \nabla h(x, u) \cdot \tau(x) \, ds$$

$$= -\oint_{e^1}^{e^2} \nabla_{\partial C_j} h(x, u) \, ds = -(h(e^2, u_j) - h(e^1, u_j)), \tag{3-3}$$

where $\tau(x)$ is the unit vector tangent to the boundary ∂C_j.

Remark 3.2. Using the discrete approximations based on Claim 3.1, if a constant value of the state variable $u(t, x) = u_j = \bar{u}$ is considered, one obtains

$$[\nabla \cdot F(x, u)]^{\text{approx}} = \frac{1}{|C_j|} \left[\oint_{\partial C_j} F(x, u) \cdot v(x) \, ds \right]^{\text{approx}}$$

$$= -\sum_{e \in \partial C_j} (h(e^2, \bar{u}) - h(e^1, \bar{u})) = 0. \tag{3-4}$$

This confirms that the discrete approximation of the divergence operator respects the divergence-free condition which is the geometric requirement that the proposed scheme should satisfy.

Reconstruction method and approximation of the one-sided local speeds of propagation of the waves. In the following, we will present the reconstruction of the proposed central-upwind scheme and the approximation used to obtain the maximum of the directional local speeds of propagation of the waves at cell interfaces inward and outward of computational cells. The semidiscrete form of the proposed scheme for (2-4) will be derived by using the approximation of the cell averages of the

solution. At each time $t = t_n$, the computed solution is

$$\boldsymbol{u}_j^n \approx \frac{1}{|C_j|} \int_{C_j} u(x, t_n) \, dV_g, \tag{3-5}$$

where $dV_g = \sqrt{g} \, dx^1 \, dx^2$.

The discrete values $\boldsymbol{u}_j^n$ of the solution at time $t = t_n$ are used to construct a conservative piecewise polynomial function with possible discontinuities at the interfaces of the computational cells C_j:

$$\tilde{u}^n(x) = \sum_j w_j^n(x) \chi_j(x), \tag{3-6}$$

where $w_j^n(x)$ is a polynomial in two variables (λ and ϕ) and χ_j is the characteristic function which is defined using the Kronecker symbol δ_{jk} and, for any point of spatial coordinate x inside the computational cell C_k, we consider $\chi_j(x) = \delta_{jk}$.

To prevent oscillations, minmod-type reconstruction can be used to obtain the polynomial function $w_j^n(x)$ for each computational cell. Page 97 describes the reconstruction method used for the proposed central-upwind scheme on the sphere.

The maximum of the directional local speeds of propagation of the waves at the k-th interface inward and outward of the computational cell C_j are denoted by a_{jk}^{in} and a_{jk}^{out}, respectively. When the solution evolves over a time step Δt, the discontinuities move inward and outward at the k-th interface of the computational cell C_j with maximum distances $a_{jk}^{\text{in}} \Delta t$ and $a_{jk}^{\text{out}} \Delta t$, respectively. These distances of propagation are used at the computational cells to delimit different areas in which the solution is still smooth and the areas in which the solution may not be smooth when it evolves from the time level t_n to t_{n+1}.

We define the domain D_j as the part inside the cell C_j in which the solution is still smooth; see Figure 1. Two other types of domains are defined: the first type includes the "rectangular" domains D_{jk}, $k = 1, 2, \ldots, m_j$, along each side of C_j of width $(a_{jk}^{\text{out}} + a_{jk}^{\text{in}}) \Delta t$ and length $l_{jk} + O(\Delta t)$, and the second type includes the domains denoted by E_{jk}, $k = 1, 2, \ldots, m_j$, around the cell vertices of computational cells. These domains are decomposed into two subdomains $D_{jk} = D_{jk}^+ \cup D_{jk}^-$ and $E_{jk} = E_{jk}^+ \cup E_{jk}^-$, where the subdomains with the superscript plus signs "$+$" and minus signs "$-$" are the domains inside and outside of the cell C_j, respectively. For purely geometrical reasons, the areas of the three types of subdomains are of orders $|D_j| = O(1)$, $|D_{jk}| = O(\Delta t)$, and $|E_{jk}| = O(\Delta t^2)$.

We consider the projection of the flux vector $\widetilde{F}$ according to the normal to the k-th cell interface $(\partial C_j)_k$:

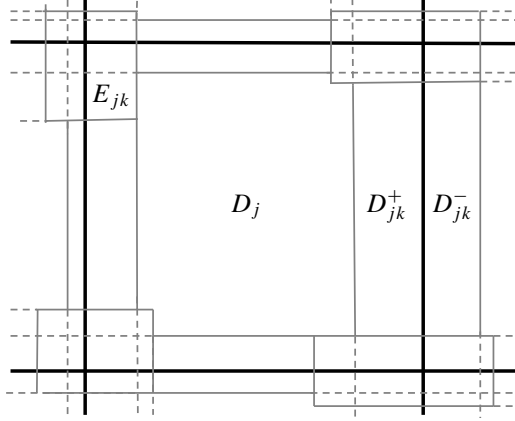$$f_{jk} = N_{jk} \cdot \widetilde{F}, \tag{3-7}$$

Figure 1. Schematic view of the decomposition of the control volume. The thick black lines are the limits of computational cells, and the thin gray lines are used for the decomposition of control volumes.

where N_{jk} is the unit normal vector to the cell interface $(\partial C_j)_k$ and $\widetilde{F}$ has the components $\sqrt{g} F^j(x, v/\sqrt{g})$ which are used in (2-8).

The one-sided local speeds of propagation of the waves at the k-th cell interface $(\partial C_j)_k$, inward and outward of the computational cell C_j, are estimated by

$$
\begin{aligned}
a_{jk}^{\text{out}} = \ & \max\left\{ \frac{\partial f_{jk}}{\partial v}(M_{jk}, u_j(M_{jk})), \frac{\partial f_{jk}}{\partial v}(M_{jk}, u_{jk}(M_{jk})), 0 \right\}, \\
a_{jk}^{\text{in}} = \ & -\min\left\{ \frac{\partial f_{jk}}{\partial v}(M_{jk}, u_j(M_{jk})), \frac{\partial f_{jk}}{\partial v}(M_{jk}, u_{jk}(M_{jk})), 0 \right\},
\end{aligned}
\tag{3-8}
$$

where $u_j(M_{jk})$ is the value of the state variable u at the midpoint M_{jk} of $(\partial C_j)_k$, which is obtained from the nonoscillatory reconstruction for the computational cell C_j and $u_{jk}(M_{jk})$ is the value of u at the same point M_{jk} using the nonoscillatory reconstruction for the neighboring cell C_{jk}.

Evolution and projection steps. In this section, the techniques used for the hyperbolic conservation laws and shallow water systems in a Cartesian framework [16; 18; 19; 15; 17; 4] will be extended to the case of hyperbolic conservation laws on the sphere. The computed cell averages $\bar{u}_j^{n+1}$ of the numerical solution at time step t_{n+1} over the computational cells C_j are used to obtain the piecewise linear reconstruction $\widetilde{w}^{n+1}$ which should satisfy the conservative requirement

$$
\bar{u}_j^{n+1} = \frac{1}{|C_j|} \int_{C_j} \widetilde{w}^{n+1}(x) \, dV_g.
\tag{3-9}
$$

The average of the function $\widetilde{w}^{n+1}$ over the domain D_j is denoted by

$$\overline{w}^{n+1}(D_j) = \frac{1}{|D_j|} \int_{D_j} \widetilde{w}^{n+1}(x) \, dV_g. \tag{3-10}$$

Note that it is possible to derive the fully discrete form of the proposed scheme but it is impractical to use and, for simplicity, we will develop the semidiscrete form of the scheme. The ODE for approximating the cell averages of the solutions is derived by letting the time step Δt go to zero. This eliminates some terms because of their orders, and we keep the more consistent terms:

$$\frac{d\overline{u}_j}{dt}(t_n) = \lim_{\Delta t \to 0} \frac{\overline{u}_j^{n+1} - \overline{u}_j^n}{\Delta t}$$

$$= \lim_{\Delta t \to 0} \frac{1}{\Delta t} \left[\frac{1}{|C_j|} \int_{D_j} \widetilde{w}^{n+1}(x) \, dV_g + \frac{1}{|C_j|} \sum_{k=1}^{m_j} \int_{D_{jk}^+} \widetilde{w}^{n+1}(x) \, dV_g \right.$$

$$\left. + \frac{1}{|C_j|} \sum_{k=1}^{m_j} \int_{E_{jk}^+} \widetilde{w}^{n+1}(x) \, dV_g - \overline{u}_j^n \right]. \tag{3-11}$$

Since the areas of domains E_{jk} with $k = 1, 2, \ldots, m_j$ are of order Δt^2, we obtain

$$\int_{E_{jk}^+} \widetilde{w}^{n+1}(x) \, dV_g = O(\Delta t^2). \tag{3-12}$$

This approximation allows us to deduce that the third term on the right-hand side of (3-11) is of order Δt^2 and the result for the limit of this term vanishes for the ODE.

The second term in (3-11), in which we use the "rectangular" domains D_{jk}^+, will be estimated by using the assumption that the spatial derivatives of $\widetilde{w}^{n+1}$ are bounded independently of Δt. Under this assumption, the following claim gives an estimation of this term with an error of order Δt^2 for each $k \in [1, m_j]$.

Claim 3.3. *Consider the reconstruction given by (3-6), its evolution $\widetilde{w}^{n+1}$ over the global domain, and the definitions given at the bottom of page 86 for the domains D_{jk} and D_{jk}^+. If we assume that the spatial derivatives of $\widetilde{w}^{n+1}$ are bounded independently of Δt, then*

$$\int_{D_{jk}^+} \widetilde{w}^{n+1}(x) \, dV_g = |D_{jk}^+| \overline{w}^{n+1}(D_{jk}) + O(\Delta t^2). \tag{3-13}$$

Proof. It is obvious that, for the cases $|D_{jk}^+| = 0$ or $|D_{jk}^-| = 0$, (3-13) is valid. We assume that $|D_{jk}^+||D_{jk}^-| \neq 0$, and we consider

$$R = \int_{D_{jk}^+} \widetilde{w}^{n+1}(x) \, dV_g - |D_{jk}^+| \overline{w}^{n+1}(D_{jk}).$$

We have

$$
\begin{aligned}
R &= \int_{D_{jk}^+} \widetilde{w}^{n+1}(x)\, dV_g - \frac{|D_{jk}^+|}{|D_{jk}|}\left(\int_{D_{jk}^+} \widetilde{w}^{n+1}(x)\, dV_g + \int_{D_{jk}^-} \widetilde{w}^{n+1}(x)\, dV_g\right) \\
&= \frac{|D_{jk}^+|}{|D_{jk}|}\left[\frac{|D_{jk}^-|}{|D_{jk}^+|}\int_{D_{jk}^+} \widetilde{w}^{n+1}(x)\, dV_g - \int_{D_{jk}^-} \widetilde{w}^{n+1}(x)\, dV_g\right] \\
&= \frac{|D_{jk}^+|}{|D_{jk}|}\left[\frac{a_{jk}^{\mathrm{out}}}{a_{jk}^{\mathrm{in}}}\int_{-a_{jk}^{\mathrm{in}}\Delta t}^{0} \widetilde{w}^{n+1}(s)\tilde{l}_{jk}\, ds - \int_{0}^{a_{jk}^{\mathrm{out}}\Delta t} \widetilde{w}^{n+1}(s)\tilde{l}_{jk}\, ds\right], \qquad \text{(3-14)}
\end{aligned}
$$

where $\tilde{l}_{jk}$ is the length of the domain D_{jk} and s is a variable along the outward axis orthogonal to the k-th cell interface; see Figures 1 and 3.

One obtains after the change of variable in the first integral of the last equality in (3-14)

$$
R = \frac{|D_{jk}^+|}{|D_{jk}|}\tilde{l}_{jk}\int_{0}^{a_{jk}^{\mathrm{out}}\Delta t}\left(\widetilde{w}^{n+1}\left(-\frac{a_{jk}^{\mathrm{in}}}{a_{jk}^{\mathrm{out}}}s\right) - \widetilde{w}^{n+1}(s)\right) ds.
$$

Using the mean value theorem on the function $\widetilde{w}^{n+1}$, we obtain

$$
R = -\frac{|D_{jk}^+|}{|D_{jk}|}\tilde{l}_{jk}\int_{0}^{a_{jk}^{\mathrm{out}}\Delta t}\frac{a^{\mathrm{in}}+a^{\mathrm{out}}}{a^{\mathrm{out}}}s\frac{\partial \widetilde{w}^{n+1}}{\partial s}(c_s)\, ds,
$$

where $c_s \in [\min(s, -sa_{jk}^{\mathrm{in}}/a_{jk}^{\mathrm{out}}), \max(s, -sa_{jk}^{\mathrm{in}}/a_{jk}^{\mathrm{out}})]$.

We denote by M the upper bound of the spatial derivative of the function $\widetilde{w}^{n+1}$ over the domain D_{jk}. Therefore,

$$
|R| \le Ml\frac{|D_{jk}^+|}{|D_{jk}^-|}\int_{0}^{a_{jk}^{\mathrm{out}}\Delta t} s\, ds = \frac{Ml}{2}|D_{jk}^+||D_{jk}^-|.
$$

Since $\tilde{l}_{jk} = l_{jk} + O(\Delta t)$ and both the areas $|D_{jk}^+|$ and $|D_{jk}^-|$ are of order Δt, we obtain $R = O(\Delta t^2)$. $\qquad\square$

Using (3-13) in Claim 3.3,

$$
\begin{aligned}
\frac{1}{|C_j|}\sum_{k=1}^{m_j}\int_{D_{jk}^+} \widetilde{w}^{n+1}(x)\, dV_g &= \frac{1}{|C_j|}\sum_{k=1}^{m_j}|D_{jk}^+|\overline{w}^{n+1}(D_{jk}) + O(\Delta t^2) \\
&= \frac{\Delta t}{|C_j|}\sum_{k=1}^{m_j}a_{jk}^{\mathrm{in}}(l_{jk}+O(\Delta t))\overline{w}^{n+1}(D_{jk}) + O(\Delta t^2). \quad \text{(3-15)}
\end{aligned}
$$

Therefore, (3-11) can be written as

$$
\frac{d\bar{u}_j}{dt}(t_n) = \lim_{\Delta t\to 0}\frac{1}{\Delta t}\left[\frac{|D_j|}{|C_j|}\overline{w}^{n+1}(D_j) - \bar{u}_j^n\right] + \sum_{k=1}^{m_j}\lim_{\Delta t\to 0}\frac{|D_{jk}^+|}{\Delta t|C_j|}\overline{w}^{n+1}(D_{jk}), \quad \text{(3-16)}
$$

where

$$\overline{w}^{n+1}(D_{jk}) = \frac{1}{|D_{jk}|} \int_{D_{jk}} \widetilde{w}^{n+1}(x)\, dV_g. \qquad (3\text{-}17)$$

In order to derive the semidiscrete form of the proposed scheme from (3-16), one needs to compute the average values $\overline{w}^{n+1}(D_{jk})$ and $\overline{w}^{n+1}(D_j)$. To compute $\overline{w}^{n+1}(D_{jk})$, (2-4) is integrated over the spacetime control volume $D_{jk} \times [t_n, t_{n+1}]$. After integration by parts and applying the divergence theorem to transform the surface integral of the divergence operator to the boundary integral and using the approximation (3-2) of the flux through the cell interfaces, we obtain

$$\overline{w}^{n+1}(D_{jk}) = \frac{1}{|D_{jk}|}\left[\int_{D_{jk}^+} w_j^n(x)\,dV_g + \int_{D_{jk}^-} w_{jk}^n(x)\,dV_g\right]$$
$$-\frac{1}{|D_{jk}|}\int_{t_n}^{t_{n+1}}\int_{D_{jk}} \nabla \cdot F(x,u)\,dV_g, \qquad (3\text{-}18)$$

and

$$\int_{D_{jk}} \nabla \cdot F(x,u)\,dV_g$$
$$= \left[\int_{\partial D_{jk}} F(x,u) \cdot v(x)\,ds\right]^{\text{approx}}$$
$$= \sum_{i=1}^{i=4} \int_{(\partial D_{jk})_i} F(x,u) \cdot v(x)\,ds$$
$$= -\left[-h(e_{jk}^2, u_j(M_{jk})) + h(e_{jk}^1, u_j(M_{jk})) + h(e_{jk}^2, u_{jk}(M_{jk})) - h(e_{jk}^1, u_{jk}(M_{jk}))\right]$$
$$+ O(\Delta t), \qquad (3\text{-}19)$$

where $(\partial D_{jk})_i$, $i = 1, 2, 3, 4$, are the four edges of the domain D_{jk}, e_{jk}^2 and e_{jk}^1 are the initial and final endpoints of the cell interface $(\partial C_j)_k$, and as mentioned before w_j^n and w_{jk}^n are the piecewise polynomial reconstructions in the computational cells C_j and C_{jk} at time t_n, respectively.

The term on the right-hand side of (3-19) of order $O(\Delta t)$ corresponds to the global result of the integration along the two edges of the domain D_{jk} having the length $(a_{jk}^{\text{in}} + a_{jk}^{\text{out}})\Delta t$ and the rest of the integration due to the difference between the length of the domain D_{jk} and the length of the cell interface $(\partial C_j)_k$.

In order to compute the spatial integrals in (3-18), Gaussian quadrature can be applied. In our case, the midpoint rule is used for simplicity:

$$\int_{D_{jk}^+} w_{jk}^n\,dV_g + \int_{D_{jk}^-} w_{jk}^n\,dV_g \approx l_{jk}\Delta t[a_{jk}^{\text{in}} u_j(M_{jk}) + a_{jk}^{\text{out}} u_{jk}(M_{jk})]. \qquad (3\text{-}20)$$

Equations (3-18), (3-19), and (3-20) lead to

$$
\lim_{\Delta t \to 0} \overline{w}^{n+1}(D_{jk}) = \frac{l_{jk}}{a_{jk}^{\text{in}} + a_{jk}^{\text{out}}} [a_{jk}^{\text{in}} u_j(M_{jk}) + a_{jk}^{\text{out}} u_{jk}(M_{jk})]
$$
$$
+ \frac{1}{a_{jk}^{\text{in}} + a_{jk}^{\text{out}}} \big[-h(e_{jk}^2, u_j(M_{jk})) + h(e_{jk}^1, u_j(M_{jk}))
$$
$$
+ h(e_{jk}^2, u_{jk}(M_{jk})) - h(e_{jk}^1, u_{jk}(M_{jk})) \big]. \quad (3\text{-}21)
$$

Therefore, we find

$$
\lim_{\Delta t \to 0} \sum_{k=1}^{m_j} \frac{|D_{jk}^+|}{\Delta t |C_j|} \overline{w}^{n+1}(D_{jk})
$$
$$
= \sum_{k=1}^{m_j} \frac{a_{jk}^{\text{in}} l_{jk}}{|C_j|(a_{jk}^{\text{in}} + a_{jk}^{\text{out}})} [a_{jk}^{\text{in}} u_j(M_{jk}) + a_{jk}^{\text{out}} u_{jk}(M_{jk})]
$$
$$
+ \sum_{k=1}^{m_j} \frac{a_{jk}^{\text{in}}}{|C_j|(a_{jk}^{\text{in}} + a_{jk}^{\text{out}})} \big[-h(e_{jk}^2, u_j(M_{jk})) + h(e_{jk}^1, u_j(M_{jk}))
$$
$$
+ h(e_{jk}^2, u_{jk}(M_{jk})) - h(e_{jk}^1, u_{jk}(M_{jk})) \big]. \quad (3\text{-}22)
$$

Now the average value $\overline{w}^{n+1}(D_j)$ will be computed. Equation (2-4) is integrated over the spacetime control volume $D_j \times [t_n, t_{n+1}]$, and after integration by parts and using the divergence theorem to transform the surface integral to a boundary integral and using (3-2), one obtains

$$
\overline{w}^{n+1}(D_j) = \frac{1}{|D_j|} \int_{D_j} w_j^n \, dV_g - \frac{1}{|D_j|} \int_{t_n}^{t_{n+1}} \int_{D_j} \nabla \cdot F(x, u) \, dV_g
$$
$$
= \frac{1}{|D_j|} \int_{D_j} w_j^n \, dV_g - \frac{\Delta t}{|D_j|} \Big(\sum_{k=1}^{m_j} [-h(e_{jk}^2, u_j(M_{jk}))
$$
$$
+ h(e_{jk}^1, u_j(M_{jk}))] + O(\Delta t) \Big). \quad (3\text{-}23)
$$

The last term in (3-23) includes $O(\Delta t)$ since e_{jk}^1 and e_{jk}^2 are corners of C_j, not D_j.

Using the previous equality,

$$
\frac{1}{\Delta t} \Big[\frac{|D_j|}{|C_j|} \overline{w}^{n+1}(D_j) - \bar{u}_j^n \Big] = \frac{1}{\Delta t} \Big\{ \frac{1}{|C_j|} \int_{D_j} w_j^n \, dV_g - \frac{\Delta t}{|C_j|} \Big(\sum_{k=1}^{m_j} [-h(e_{jk}^2, u_j(M_{jk}))
$$
$$
+ h(e_{jk}^1, u_j(M_{jk}))] + O(\Delta t) \Big) - \bar{u}_j^n \Big\}, \quad (3\text{-}24)
$$

which leads to

$$\lim_{\Delta t \to 0} \frac{1}{\Delta t}\left[\frac{|D_j|}{|C_j|}\bar{w}^{n+1}(D_j) - \bar{u}_j^n\right] = -\frac{1}{|C_j|}\sum_{k=1}^{m_j} a_{jk}^{\text{in}} l_{jk} u_j(M_{jk})$$

$$-\frac{1}{|C_j|}\sum_{k=1}^{m_j}[-h(e_{jk}^2, u_j(M_{jk})) + h(e_{jk}^1, u_j(M_{jk}))]. \quad (3\text{-}25)$$

Equations (3-22) and (3-25) are used together to obtain the semidiscrete form

$$\frac{d\bar{u}_j}{dt} = -\frac{1}{|C_j|}\sum_{k=1}^{m_j} a_{jk}^{\text{in}} l_{jk} u_j(M_{jk}) - \frac{1}{|C_j|}\sum_{k=1}^{m_j}[-h(e_{jk}^2, u_j(M_{jk})) + h(e_{jk}^1, u_j(M_{jk}))]$$

$$+ \sum_{k=1}^{m_j}\frac{a_{jk}^{\text{in}} l_{jk}}{|C_j|(a_{jk}^{\text{in}} + a_{jk}^{\text{out}})}[a_{jk}^{\text{in}} u_j(M_{jk}) + a_{jk}^{\text{out}} u_{jk}(M_{jk})]$$

$$+ \sum_{k=1}^{m_j}\frac{a_{jk}^{\text{in}}}{|C_j|(a_{jk}^{\text{in}} + a_{jk}^{\text{out}})}\Big[-h(e_{jk}^2, u_j(M_{jk})) + h(e_{jk}^1, u_j(M_{jk}))$$

$$+ h(e_{jk}^2, u_{jk}(M_{jk})) - h(e_{jk}^1, u_{jk}(M_{jk}))\Big]. \quad (3\text{-}26)$$

This equation can be rewritten in the form

$$\frac{d\bar{u}_j}{dt} = \frac{1}{|C_j|}\sum_{k=1}^{m_j}\frac{a_{jk}^{\text{in}} a_{jk}^{\text{out}} l_{jk}}{a_{jk}^{\text{in}} + a_{jk}^{\text{out}}}(u_{jk}(M_{jk}) - u_j(M_{jk}))$$

$$+ \frac{a_{jk}^{\text{in}} a_{jk}^{\text{out}}}{|C_j|(a_{jk}^{\text{in}} + a_{jk}^{\text{out}})}\Big\{a_{jk}^{\text{in}}[h(e_{jk}^2, u_j(M_{jk})) - h(e_{jk}^1, u_j(M_{jk}))]$$

$$+ a_{jk}^{\text{out}}[h(e_{jk}^2, u_{jk}(M_{jk})) - h(e_{jk}^1, u_{jk}(M_{jk}))]\Big\}, \quad (3\text{-}27)$$

which can be rewritten as

$$\frac{d\bar{u}_j}{dt} = -\frac{1}{|C_j|}\sum_{k=1}^{m_j}\frac{a_{jk}^{\text{in}} \boldsymbol{H}(u_{jk}(M_{jk})) + a_{jk}^{\text{out}} \boldsymbol{H}(u_j(M_{jk}))}{a_{jk}^{\text{in}} + a_{jk}^{\text{out}}}$$

$$+ \frac{1}{|C_j|}\sum_{k=1}^{m_j}\frac{a_{jk}^{\text{in}} a_{jk}^{\text{out}} l_{jk}}{a_{jk}^{\text{in}} + a_{jk}^{\text{out}}}[u_{jk}(M_{jk}) - u_j(M_{jk})], \quad (3\text{-}28)$$

where $\boldsymbol{H}(u_j(M_{jk}))$ and $\boldsymbol{H}(u_{jk}(M_{jk}))$ are given by

$$\begin{aligned}\boldsymbol{H}(u_j(M_{jk})) &= -[h(e_{jk}^2, u_j(M_{jk})) - h(e_{jk}^1, u_j(M_{jk}))], \\ \boldsymbol{H}(u_{jk}(M_{jk})) &= -[h(e_{jk}^2, u_{jk}(M_{jk})) - h(e_{jk}^1, u_{jk}(M_{jk}))].\end{aligned} \quad (3\text{-}29)$$

The function $\boldsymbol{H}$ is defined in the form (3-29) in order to be consistent with the total approximate flux through the cell interface as presented by (3-2) in Claim 3.1.

Remark 3.4. If the value of $a_{jk}^{\mathrm{in}} + a_{jk}^{\mathrm{out}}$ in (3-28) is zero or very close to zero (smaller than 10^{-8} in our numerical experiments), we avoid division by zero or by a very small number using the following approximations

$$\frac{a_{jk}^{\mathrm{in}}\boldsymbol{H}(u_{jk}(M_{jk})) + a_{jk}^{\mathrm{out}}\boldsymbol{H}(u_j(M_{jk}))}{a_{jk}^{\mathrm{in}} + a_{jk}^{\mathrm{out}}} \approx \frac{1}{2}\left[\sum_{k=1}^{m_j}\boldsymbol{H}(u_j(M_{jk})) + \sum_{k=1}^{m_j}\boldsymbol{H}(u_{jk}(M_{jk}))\right],$$

$$\frac{a_{jk}^{\mathrm{in}}a_{jk}^{\mathrm{out}}}{|C_j|(a_{jk}^{\mathrm{in}} + a_{jk}^{\mathrm{out}})}\sum_{k=1}^{m_j} l_{jk}[u_{jk}(M_{jk}) - u_j(M_{jk})] \approx 0. \qquad (3\text{-}30)$$

These approximations are obtained using similar extreme distances of the propagation of the waves at the cell interface inward and outward of the computational cell to define the domains D_j, D_{jk}, and E_{jk}. The semidiscretization (3-28) and (3-29) is a system of ODEs which has to be integrated in time using an accurate and stable temporal scheme. In our numerical examples reported in Section 6, we used the third-order total-variation diminishing Runge–Kutta method.

The geometry-compatible condition. In the semidiscrete form (3-28) and (3-29) of the proposed scheme, if we consider a constant value of the function $u \equiv \bar{u}$, the second term in the right-hand side of (3-28) vanishes. For this constant function, we obtain for each interface cell k

$$u_j(M_{jk}) = u_{jk}(M_{jk}) = \bar{u} \qquad (3\text{-}31)$$

and

$$\boldsymbol{H}(u_j(M_{jk})) = \boldsymbol{H}(u_{jk}(M_{jk})). \qquad (3\text{-}32)$$

The first term in the right-hand side of (3-28) becomes

$$-\frac{1}{|C_j|}\sum_{k=1}^{m_j}\frac{a_{jk}^{\mathrm{in}}\boldsymbol{H}(u_{jk}(M_{jk})) + a_{jk}^{\mathrm{out}}\boldsymbol{H}(u_j(M_{jk}))}{a_{jk}^{\mathrm{in}} + a_{jk}^{\mathrm{out}}} = -\frac{1}{|C_j|}\sum_{k=1}^{m_j}\boldsymbol{H}(u_j(M_{jk})).$$
$$(3\text{-}33)$$

Since we have

$$\sum_{k=1}^{m_j}\boldsymbol{H}(u_j(M_{jk})) = \sum_{k=1}^{m_j}\boldsymbol{H}(u_{jk}(M_{jk})) = -\sum_{k=1}^{m_j}[h(e_{jk}^2, \bar{u}) - h(e_{jk}^1, \bar{u})] = 0, \quad (3\text{-}34)$$

we conclude that the first term on the right-hand side of (3-28) will be canceled, which confirms that the proposed scheme respects the geometry-compatibility condition.

Remark 3.5. In the formulation of the proposed central-upwind finite volume method, the midpoint rule is used to compute the spatial integrals. The proposed scheme is second-order accurate, and we obtain the error in the form $E \sim C(\Delta x)^2$ where the magnitude of the constant C is also important as well as the order of
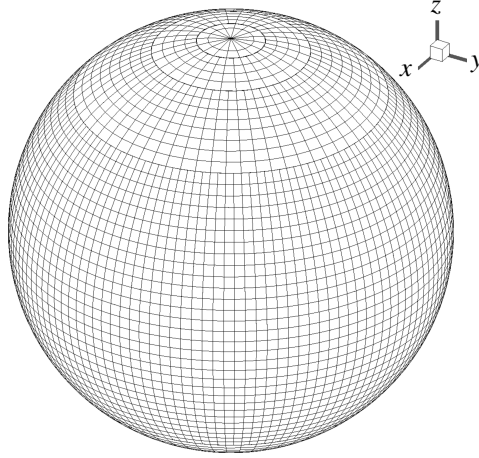
Figure 2. Type of grid used on the sphere.

accuracy of the scheme [30]. For the same second-order accuracy of the proposed schemes using Gaussian quadrature and the midpoint rule, the parameter C obtained using Gaussian quadrature is small in comparison to the value obtained for the case using the midpoint rule. The use of Gaussian quadrature will improve the accuracy of the scheme compared to the midpoint rule. Gaussian quadrature will not have any impact on the geometry-compatibility condition of the proposed scheme.

4. Formulation using the latitude-longitude grid on the sphere

Computational grid on the sphere. The geometry-compatible scheme was developed in the previous section for scalar nonlinear hyperbolic conservation laws using a general grid on the sphere. However, in order to prevent oscillations, an appropriate piecewise linear reconstruction should be proposed according to the computational grid used in the proposed method. In the following, we will describe the computational grid and the nonoscillatory piecewise linear reconstruction used in our numerical experiments. The position of each point on the sphere can be represented by its longitude $\lambda \in [0, 2\pi]$ and its latitude $\phi \in [-\pi/2, \pi/2]$. The grid considered in our numerical examples is shown in Figure 2. The coordinates are singular at the south and north poles, corresponding to $\phi = -\pi/2$ and $\phi = \pi/2$, respectively. The Cartesian coordinates are denoted by $x = (x_1, x_2, x_3)^T \in \mathbb{R}^3$ for standard orthonormal basis vectors $\boldsymbol{i}_1, \boldsymbol{i}_2$, and $\boldsymbol{i}_3$.

The unit tangent vectors in the directions of longitude and latitude at each point x on the sphere with coordinates (λ, ϕ) are given by

$$\boldsymbol{i}_\lambda = -(\sin \lambda)\boldsymbol{i}_1 + (\cos \lambda)\boldsymbol{i}_2,$$
$$\boldsymbol{i}_\phi = -(\sin \phi)(\cos \lambda)\boldsymbol{i}_1 - (\sin \phi)(\sin \lambda)\boldsymbol{i}_2 + (\cos \phi)\boldsymbol{i}_3. \tag{4-1}$$
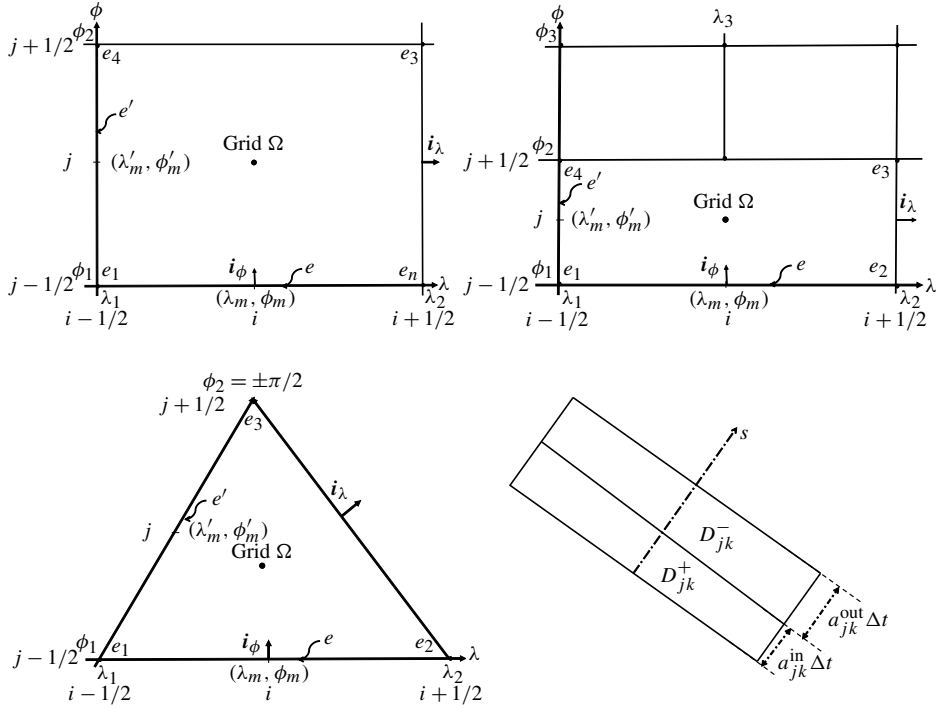
Figure 3. Types of grids used on the sphere. Bottom right: the domain $D_{jk} = D_{jk}^+ \cup D_{jk}^-$.

The unit normal vector to the sphere at the same point $x \in \mathbb{S}^2$ is given by

$$n(x) = (\cos\phi)(\cos\lambda)\mathbf{i}_1 + (\cos\phi)(\sin\lambda)\mathbf{i}_2 + (\sin\phi)\mathbf{i}_3. \qquad (4\text{-}2)$$

In spherical coordinates, for any vector field F represented by $F = F_\lambda \mathbf{i}_\lambda + F_\phi \mathbf{i}_\phi$, the equation of conservation law (2-4) can be rewritten as

$$\partial_t u + \frac{1}{\cos\phi}\left(\frac{\partial}{\partial\phi}(F_\phi \cos\phi) + \frac{\partial F_\lambda}{\partial\lambda}\right) = 0. \qquad (4\text{-}3)$$

The three general structures of the computational cells used as part of the discretization grid on the sphere are shown in Figure 3. When we go from the equator to the north or south poles, the cells are changed by a ratio of 2 at some special latitude circles to reduce the number of cells in order to satisfy the stability condition and to ensure consistency of precision in the entire domain of the sphere. For the stability condition, the CFL number defined as the maximum of the ratio $v_j \Delta t / L_j$ is used. The parameter $v_j = \max_k(a_{jk}^{\text{out}}, a_{jk}^{\text{in}})$ is the maximum of the directional local speeds of propagation of the waves, and L_j is the minimum length of the computational cell C_j in the longitude and latitude directions. The domain of each cell Ω is defined as $\Omega = \{(\lambda, \phi) : \lambda_1 \leq \lambda \leq \lambda_2, \ \phi_1 \leq \phi \leq \phi_2\}$. Near the north or south poles, a "triangular" cell is considered which is a special case of the standard "rectangular" cell shown in Figure 3 with zero length for the side located on the pole.

A nonoscillatory piecewise linear reconstruction. In this section, we describe the piecewise linear reconstruction used in the proposed scheme. For simplicity, in the notations, we will use the indices i and j for the cell centers along the longitude and latitude, respectively (see Figure 3). At each time step t_n, data cell average values $u_{i,j}^n$ in each cell of center (λ_i, ϕ_j) are locally replaced by a piecewise linear function. The obtained reconstruction is

$$u_{i,j}^n(\lambda, \phi) = u_{i,j}^n + (\lambda - \lambda_i)\mu_{i,j}^n + (\phi - \phi_j)\sigma_{i,j}^n, \tag{4-4}$$

where $\mu_{i,j}^n$ and $\sigma_{i,j}^n$ are the slopes in the directions of longitude and latitude, respectively. To prevent oscillations, we propose the following minmod-type reconstruction to obtain the slopes in the longitude and latitude directions:

$$\mu_{i,j}^n = \text{minmod}\left[\frac{u_{i+1,j}^n - u_{i,j}^n}{\lambda_{i+1} - \lambda_i}, \frac{u_{i+1,j}^n - u_{i-1,j}^n}{\lambda_{i+1} - \lambda_{i-1}}, \frac{u_{i,j}^n - u_{i-1,j}^n}{\lambda_i - \lambda_{i-1}}\right],$$
$$\sigma_{i,j}^n = \text{minmod}\left[\frac{u_{i,j+1}^n - u_{i,j}^n}{\phi_{j+1} - \phi_j}, \frac{u_{i,j+1}^n - u_{i,j-1}^n}{\phi_{j+1} - \phi_{j-1}}, \frac{u_{i,j}^n - u_{i,j-1}^n}{\phi_j - \phi_{j-1}}\right], \tag{4-5}$$

where the minmod function is defined as

$$\text{minmod}(\kappa_1, \kappa_2, \kappa_3)$$
$$= \begin{cases} \kappa \min(|\kappa_1|, |\kappa_2|, |\kappa_3|) & \text{if } \kappa = \text{sign}(\kappa_1) = \text{sign}(\kappa_2) = \text{sign}(\kappa_3), \\ 0 & \text{otherwise.} \end{cases} \tag{4-6}$$

At each step, we compute the average values of the state variable u in the computational cells. The same values are used as the values of u at the cell centers of coordinates (λ_i, ϕ_j). The suitable points, inside the cells which respect these conditions for the linear reconstruction used in this study, should have the spherical coordinates

$$\lambda_i = \frac{\lambda_1 + \lambda_2}{2},$$
$$\phi_j = \frac{\phi_2 \sin(\phi_2) - \phi_1 \sin(\phi_1) + \cos\phi_2 - \cos\phi_1}{\sin\phi_2 - \sin\phi_1}, \tag{4-7}$$

where λ_1, λ_2, ϕ_1, and ϕ_2 correspond to the longitude and latitude coordinates of the cell nodes as shown in Figure 3.

5. Geometry-compatible flux vectors and particular solutions of interest

Classes of geometry-compatible flux vectors. We have introduced, in [3], two classes of flux vector fields for (2-9). In this classification, the structure of the potential function $h(x, u)$ was used to distinguish between *foliated* and *generic* fluxes. In the proposed classification, the parametrized level sets defined by $\Gamma_{C,u} = \{x \in \mathbb{R}^3 : h(x, u) = C\}$, where $C \in \mathbb{R}$, are used for the flux vector $F(x, u) =$

$n(x) \wedge \nabla h(x, u)$ associated to the potential function h. The flux F is called a *foliated flux field* if the associated family of level sets $\{\Gamma_{C,u}\}_{C \in \mathbb{R}}$ in $\mathbb{R}^3$ is independent of the state variable u. In other words, for any two parameters u_1 and u_2, one can find two real numbers C_1 and C_2 such that $\Gamma_{C_1, u_1} = \Gamma_{C_2, u_2}$. For the generic flux field, the potential function $h = h(x, u)$ does not have this structure.

The dependency of the potential function on the space variable x generates the propagation of the waves, while the dependency on the state variable u leads to the formation of shocks in the solutions. The foliated flux with linear behavior generates the spatially periodic solutions while the foliated flux with nonlinear behavior can generate nontrivial stationary solutions. In our analysis in [3], we have concluded that the new classification introduced and the character of linearity of the flux are sufficient to predict the late-time asymptotic behavior of the solutions. For a linear foliated flux, the solutions are simply transported along the level sets. The generic flux generates large variations in solutions, which converge to constant values within independent domains on the sphere. For the nonlinear foliated flux, the solution converges to its constant average in each level set. For this flux, any steady state solution should be constant along each level set. This type of nontrivial stationary solutions are used in our numerical experiments to demonstrate the performance of the proposed central-upwind finite volume method.

Particular solutions of interest. The nontrivial steady state solutions which will be used in our numerical experiments are obtained using nonlinear foliated fluxes. We are particularly interested in nonlinear foliated fluxes based on a scalar potential function of the form

$$h(x, u) = \varphi(x \cdot a) f(u), \tag{5-1}$$

where $x \cdot a$ denotes the scalar product of the vector x and some constant vector $a = (a_1, a_2, a_3)^T \in \mathbb{R}^3$, while f is a function of the state variable u and φ is a function of one variable. This scalar potential function leads to the gradient-type flux vector field $\Phi(x, u) = \varphi'(x \cdot a) f(u) a$, where φ' is the derivative of the function φ. The flux is obtained using (2-2) as

$$F(x, u) = \varphi'(x \cdot a) f(u) n(x) \wedge a. \tag{5-2}$$

For this foliated flux vector and any function $\tilde{u}$ which depends on one variable, the function defined as $u_0(x) = \tilde{u}(x \cdot a) = \tilde{u}(a_1 x_1 + a_2 x_2 + a_3 x_3)$ is a steady state solution to the conservation law (2-9) associated to the flux vector $F(x, u)$. Arbitrary functions φ and values of the vector a are used to construct nonlinear foliated fluxes and the corresponding nontrivial stationary solutions. In the following, ∇ will be used as the standard gradient operator defined using the variable x and, if other variables are used, they will be specified in the notation by ∇_y for the gradient operator using any other variable y.

In order to prove that the function $u_0(x)$ is a steady state solution of (2-9), the Claim 3.2 in [5] will be used. This claim states that, for any smooth function $h(x, u)$ defined on $\mathbb{S}^2$ with the associated gradient $\Phi = \nabla h$, if the function u_0 defined on $\mathbb{S}^2$ satisfies the condition $\nabla_y h(y, u_0(x))_{|y=x} = \nabla H(x)$, where H is a smooth function defined in a neighborhood of $\mathbb{S}^2$, then the function u_0 is a steady state solution of the conservation law (2-9) associated to the flux vector $F(x, u) = n(x) \wedge \Phi(x, u)$. This result will be used to prove the following corollary related to nontrivial stationary solutions which are obtained using the nonlinear foliated flux vectors.

Claim 5.1 (a family of steady state solutions). *Consider the foliated flux vector $F(x, u) = n(x) \wedge \Phi(x, u)$ with $\Phi = \nabla h$ and $h(x, u) = \varphi(x \cdot a) f(u)$, where $a = (a_1, a_2, a_3)^T \in \mathbb{R}^3$, f is a function of the state variable u, and the function φ depends on one variable. For any function $\tilde{u}$ which depends on one variable, the function defined as $u_0(x) = \tilde{u}(x \cdot a) = \tilde{u}(a_1 x_1 + a_2 x_2 + a_3 x_3)$ is a steady state solution to the conservation law (2-9) associated to the flux $F(x, u)$.*

Proof. We consider the function

$$H(x) = H_0(a_1 x_1 + a_2 x_2 + a_3 x_3), \tag{5-3}$$

where H_0 is defined by

$$H_0(\mu) = \int_{\mu_0}^{\mu} \varphi'(\mu) f(\tilde{u}(\mu)) \, d\mu, \tag{5-4}$$

for some reference value μ_0.

The function $h(x, u) = \varphi(x \cdot a) f(u)$ is smooth in $\mathbb{R}^3$, and one obtains

$$\nabla_y h(y, u_0(x))_{|y=x} = \varphi'(x \cdot a) f(\tilde{u}(x \cdot a)) \sum_{k=1}^{k=3} a_k i_k, \tag{5-5}$$

which leads to

$$\nabla_y h(y, u_0(x))_{|y=x} = \nabla H(x). \tag{5-6}$$

As mentioned before, according to Claim 3.2 in [5], the condition (5-6) is sufficient to conclude that the function $u_0(x)$ is a steady state solution of the conservation law (2-9). $\square$

We will consider the nonlinear foliated flux vectors based on the scalar potential functions of the form $h(x, u) = \varphi(x_1) f(u)$, where the function φ is not constant. For this flux, any nonconstant function which depends on x_1 only is a nontrivial steady state solution of (2-9). Another form of nonlinear foliated flux is used in our numerical tests which is obtained by using the scalar potential function of the form $h(x, u) = \varphi(x_1 + x_2 + x_3) f(u)$. This case leads to steady state solutions of the form $u_0(x) = \tilde{u}(x_1 + x_2 + x_3)$. In this paper we will consider discontinuous steady state solutions to test the performance of the proposed central-upwind method. Claim 5.1

will be used to obtain discontinuous steady state solutions for some particular flux vector fields. We will use the nonlinear foliated flux vectors which are obtained by using the scalar potential function of the form $h(x, u) = \varphi(x \cdot a) f(u)$, where $f(u) = u^2/2$. For these flux vectors, the function defined as $u_0(x) = \chi(x \cdot a) \tilde{u}(x \cdot a)$ is a discontinuous stationary solution of (2-9), where $\chi(x \cdot a) = \pm 1$.

In Tests 7 and 8, the proposed central-upwind scheme is employed to compute *confined solutions* of the conservation law (2-9). In these cases, we consider the flux vector $F(x, u)$ which vanishes outside a domain Θ in the sphere $\mathbb{S}^2$. If the initial condition $u_0(x)$ vanishes outside of Θ, then the solution should vanish outside the domain Θ for all time. However, the solution can evolve inside the domain Θ depending on the type of flux and the initial condition considered inside of Θ. This case is observed in Test 7 presented in Section 6, where we choose the initial condition which is not stationary inside the domain Θ but vanishes outside this domain. In Test 8, we will consider the flux vector $F(x, u)$ which vanishes outside Θ and is defined inside this domain using the scalar potential function $h(x, u) = \varphi(x \cdot a) f(u)$. This leads to a flux vector F which satisfies the conditions mentioned in Claim 5.1. For this case, we will consider an initial condition of the form $u_0(x) = \tilde{u}(x \cdot a)$ inside a domain Θ and that vanishes outside this domain. The solution should be stationary inside Θ and should vanish outside this domain.

6. Numerical experiments

In this section, we demonstrate the performance of the proposed central-upwind scheme on a variety of numerical examples. Different types of nonlinear foliated fluxes are used to construct some particular and interesting solutions. In Example 6.1, four numerical tests are performed using different discontinuous steady state solutions of the conservation law (2-9) with the nonlinear foliated flux vectors based on the scalar potential functions of the form $h(x, u) = \varphi(x_1) f(u)$. In Example 6.2, two numerical tests are performed using different discontinuous steady state solutions in the spherical cap of (2-9) which are obtained by using the nonlinear foliated flux corresponding to the scalar potential function of the form $h(x, u) = \varphi(x_1 + x_2 + x_3) f(u)$. In Example 6.3, two numerical tests are performed where the proposed scheme is employed to compute confined solutions.

Example 6.1 (discontinuous steady state solutions). First, we consider the potential function $h(x, u) = x_1 f(u)$, where $f(u) = u^2/2$, which leads to the nonlinear foliated flux vector $F(x, u) = f(u) n(x) \wedge i_1$. We take the following discontinuous steady state solution of (2-9) as initial condition (Test 1):

$$u_2(x) = \begin{cases} \gamma x_1^3 & \text{if } -1 \leq x_1 \leq 0.5, \\ -\gamma x_1^2/(2x_1 + 1) & \text{if } 0.5 \leq x_1 \leq 1, \end{cases} \tag{6-1}$$
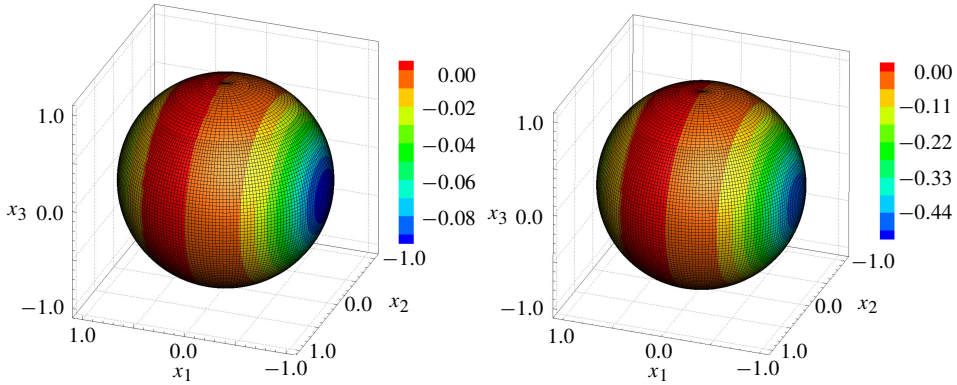
Figure 4. Solutions on the entire sphere at time $t = 5$ for Test 1 (left) and Test 2 (right).

where γ is an arbitrary constant which controls the amplitude and shocks of the solution. This solution has a single closed curve of discontinuity on the sphere.

The numerical solution is computed using a grid with an equatorial longitude step $\Delta\lambda = \pi/96$ and a latitude step $\Delta\phi = \pi/96$ and CFL $= 0.1$. Figure 4, left, shows the numerical solution with $\gamma = 0.1$ which is computed using the proposed scheme at a global time $t = 5$. The numerical solution remains nearly unchanged in time using the proposed scheme. The numerical solution error defined by using the L^2 norm is computed by summation over all grid cells on the sphere. For Test 1, the error is $u_{\text{error}} = 1.5 \times 10^{-4}$ at time $t = 5$, which is small compared to the full range of the numerical solution $u_{\max} - u_{\min} = 0.1$.

Another test is performed using the steady state solution (6-1) as the initial condition with $\gamma = 0.5$ (Test 2) and the same computational grid used in Test 1 and CFL $= 0.6$. As shown in Figure 4, right, the solution remains nearly unchanged up to a global time $t = 5$. The error using the L^2 norm is $u_{\text{error}} = 2.7 \times 10^{-3}$, which is small compared to the full range of the solution $u_{\max} - u_{\min} = 0.5$.

Now we consider a new test (Test 3) using the following steady state solution, with more discontinuities, which is defined in three domains separated by two closed curves on the sphere:

$$u_2(x) = \begin{cases} \gamma x_1^4 & \text{if} \quad -1 \le x_1 \le -0.5, \\ 0.5\gamma x_1^3 & \text{if} \ -0.5 < x_1 < 0.5, \\ -0.25\gamma x_1^2 & \text{if} \quad 0.5 \le x_1 \le 1. \end{cases} \qquad (6\text{-}2)$$

The numerical solution is computed using CFL $= 0.1$ and the same grid on the sphere used in the previous tests. As shown in Figure 5, left, the numerical solution which is obtained at time $t = 5$ using the proposed method based on the initial condition (6-2) with $\gamma = 0.1$ remains nearly unchanged. The error is $u_{\text{error}} = 9.6 \times 10^{-5}$, which is small compared to the full range $u_{\max} - u_{\min} = 0.1$.
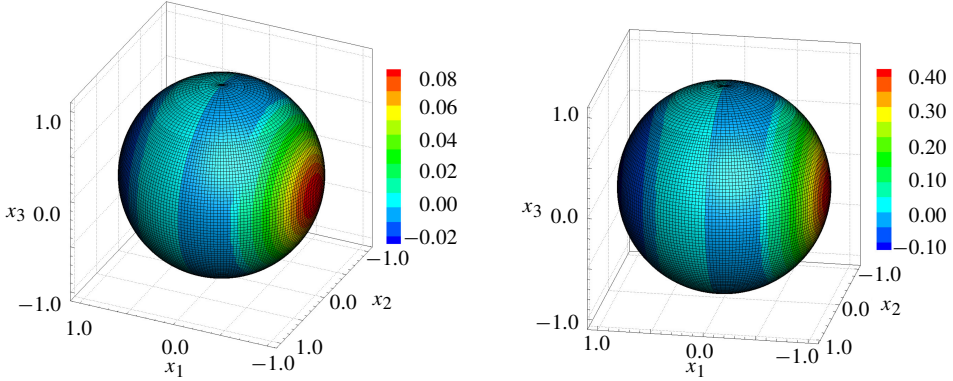
Figure 5. Solutions on the entire sphere at time $t = 5$ for Test 3 (left) and Test 4 (right).

For $\gamma = 0.5$ (Test 4), we used the same computational grid and CFL $= 0.6$. As is shown in Figure 5, right, again for this test the numerical solution at time $t = 5$ remains nearly unchanged. The error using the L^2 norm is $u_{\text{error}} = 1.9 \times 10^{-3}$, which is small compared to the full range of the solution $u_{\max} - u_{\min} = 0.6$.

Example 6.2 (discontinuous steady state solutions in a spherical cap). In the following, the performance of the proposed finite volume method will be analyzed using some particular steady state solutions in a spherical cap. The scalar potential function $h(x, u) = (x_1 + x_2 + x_3) f(u)$ is considered with $f(u) = u^2/2$. This leads to the nonlinear foliated flux $F(x, u) = f(u)n(x) \wedge (i_1 + i_2 + i_3)$. The function of the form $u(x) = \chi(\theta)\tilde{u}(\theta)$ is a steady state solution of (2-9), where $\tilde{u}$ is an arbitrary real function depending on one variable and $\theta = x_1 + x_2 + x_3$. In this numerical example (Test 5), the following discontinuous steady state solution is considered as the initial condition:

$$u(0, x) = \begin{cases} 0.1/(\theta + 2) & \text{if } 0 \le \theta, \\ -0.1/(\theta - 2) & \text{otherwise.} \end{cases} \tag{6-3}$$

The numerical solution is computed by using a grid with an equatorial longitude step $\Delta\lambda = \pi/96$ and a latitude step $\Delta\phi = \pi/96$ and CFL $= 0.1$. Figure 6, left, shows the numerical solution, which remains nearly unchanged in time after being subjected to integration up to a global time $t = 5$ by the proposed scheme. The numerical solution error defined by using the L^2 norm is $u_{\text{error}} = 1.3 \times 10^{-3}$, which is small compared to the full range $u_{\max} - u_{\min} = 0.1$. The following numerical example (Test 6) is performed using the same nonlinear foliated flux considered in Test 5 and the steady state solution with more discontinuities defined by

$$u(0, x) = \begin{cases} 0.2\theta^3 & \text{if } 0.5 \le \theta, \\ 0.1\theta^2 & \text{if } \theta \le -0.5, \\ -0.025 & \text{otherwise.} \end{cases} \tag{6-4}$$
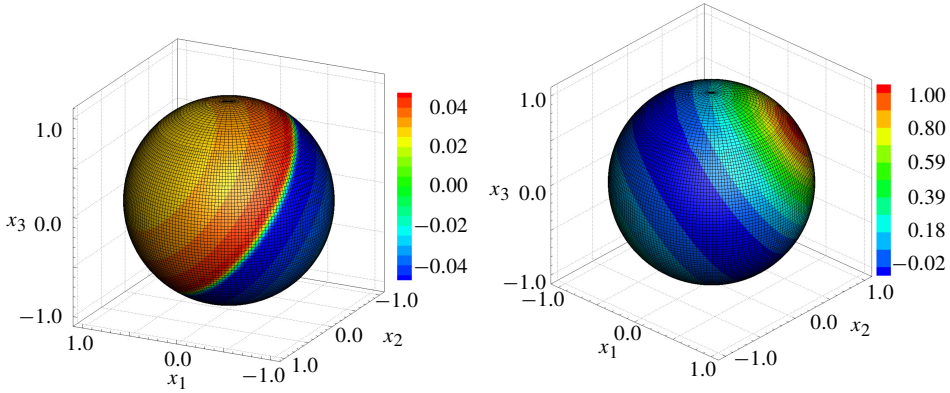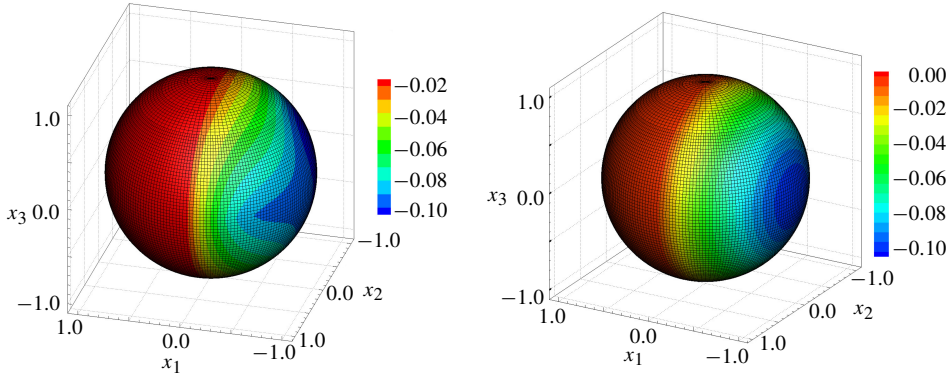
Figure 6. Solutions on the entire sphere at time $t = 5$ for Test 5 (left) and Test 6 (right).

The numerical solution is computed using the same grid used in Test 5 and CFL $= 0.9$. Figure 6, right, shows the numerical solution at time $t = 5$, which remains stationary with the error $u_{\text{error}} = 1.8 \times 10^{-3}$, negligible compared to the full range of the solution $u_{\max} - u_{\min} = 1.06$.

Example 6.3 (confined solutions). In this part, two numerical tests are performed using confined solutions of the conservation law (2-9) based on the flux vector which is obtained using the potential function

$$h(x, u) = \begin{cases} x_1^2 f_1(u) & \text{if } x_1 \leq 0, \\ 0 & \text{otherwise.} \end{cases} \tag{6-5}$$

In Test 7, we consider the function

$$u(x, 0) = \begin{cases} 0.1(1 + x_2^2)x_1 & \text{if } x_1 \leq 0, \\ 0 & \text{otherwise.} \end{cases} \tag{6-6}$$

The solution of the conservation law (2-9), which is obtained using the function (6-6) as the initial condition, is confined, and it vanishes outside the domain $x_1 \leq 0$. The numerical solution is computed using the proposed scheme with an equatorial longitude step $\Delta\lambda = \pi/96$, a latitude step $\Delta\phi = \pi/96$, and CFL $= 0.1$. Figure 7, left, shows the numerical solution at time $t = 5$. The solution evolves in time inside the domain $x_1 \leq 0$, but it vanishes outside this domain, which is in good agreement with the evolution of the analytical solution.

In the second numerical test (Test 8), we consider an initial condition which is a confined solution and steady state inside the domain $x_1 \leq 0$. The following initial condition is considered:

$$u(x, 0) = \begin{cases} 0.1x_1 & \text{if } x_1 \leq 0, \\ 0 & \text{otherwise.} \end{cases} \tag{6-7}$$

Figure 7. Solutions on the entire sphere at time $t = 5$ for Test 7 (left) and Test 8 (right)

The numerical solution is computed using the proposed central-upwind scheme with the same grid and CFL number which are used in Test 7. Figure 7, right, shows the numerical solution at time $t = 5$. The solution remains steady state in the domain $x_1 \leq 0$, and it vanishes outside this domain for all time as does the initial condition, which is in good agreement with the evolution of the analytical solution. The L^2 error of the numerical solution over the sphere is $u_{\text{error}} = 9.6 \times 10^{-5}$ at time $t = 5$, which is small compared to the full range of the solution $u_{\text{max}} - u_{\text{min}} = 0.1$.

7. Concluding remarks

We have introduced a new geometry-preserving, central-upwind scheme for the discretization of hyperbolic conservation laws posed on the sphere. The main advantage of the proposed scheme is its simplicity since it does not use any Riemann solver and, moreover, the semidiscrete form of our scheme is strongly connected to the geometry of the sphere. The use of Gaussian quadrature will improve the accuracy of the proposed method compared to the midpoint rule using the same computational grid. The Gaussian quadrature does not have an impact on the geometry-compatibility condition of the scheme.

A nonoscillatory reconstruction is used in which the gradient of each variable is computed using a minmod function in order to ensure stability. Our numerical experiments demonstrate the ability of the proposed scheme to avoid oscillations. The performance of the second-order version was tested using relevant numerical examples, and the results clearly demonstrated the scheme's potential and its ability to resolve discontinuous solutions to conservation laws posed on a curved geometry.

We observe that the formulation of the semidiscrete formulation is based on some approximations and assumptions. The scheme is more suitable for discontinuous solutions with shocks of average amplitude. However, the proposed method has the advantage of simplicity compared to the class of upwind schemes. As previously

mentioned, the first advantage is that the proposed scheme is free of any Riemann solver. The second advantage is related to the resolution: we do not use the splitting approach which is often applied in upwind schemes as a simplification technique in order to be able to solve the Riemann problems. This again renders the proposed numerical scheme less expensive compared to upwind methods.

The scheme we have developed here for nonlinear hyperbolic conservation laws could be extended to multidimensional hyperbolic conservation laws and to shallow water models posed on the sphere by extending the methodology in [4; 7] in which central-upwind schemes for solving two-dimensional Cartesian systems for shallow water models were designed. For shallow water systems, instead of the geometric compatibility condition used in the present study, the so-called *C*-property related to stationary solutions and introduced in [38] should be used in designing a well-balanced central-upwind scheme.

Acknowledgments

References

[1] P. Amorim, M. Ben-Artzi, and P. G. LeFloch, *Hyperbolic conservation laws on manifolds: total variation estimates and the finite volume method*, Methods Appl. Anal. **12** (2005), no. 3, 291–323.

[2] P. Amorim, P. G. LeFloch, and B. Okutmustur, *Finite volume schemes on Lorentzian manifolds*, Commun. Math. Sci. **6** (2008), no. 4, 1059–1086.

[3] A. Beljadid, P. G. LeFloch, and A. Mohammadian, *A geometry-preserving finite volume method for conservation laws on curved geometries*, preprint, 2013.

[4] A. Beljadid, A. Mohammadian, and A. Kurganov, *Well-balanced positivity preserving cell-vertex central-upwind scheme for shallow water flows*, Comput. Fluids **136** (2016), 193–206.

[5] M. Ben-Artzi, J. Falcovitz, and P. G. LeFloch, *Hyperbolic conservation laws on the sphere: a geometry-compatible finite volume scheme*, J. Comput. Phys. **228** (2009), no. 16, 5650–5668.

[6] M. Ben-Artzi and P. G. LeFloch, *Well-posedness theory for geometry-compatible hyperbolic conservation laws on manifolds*, Ann. Inst. H. Poincaré (C) **24** (2007), no. 6, 989–1008.

[7] S. Bryson, Y. Epshteyn, A. Kurganov, and G. Petrova, *Well-balanced positivity preserving central-upwind scheme on triangular grids for the Saint-Venant system*, ESAIM Math. Model. Numer. Anal. **45** (2011), no. 3, 423–446.

[8] T. Ceylan, P. G. LeFloch, and B. Okutmustur, *The relativistic Burgers equation on a FLRW background and its finite volume approximation*, preprint, 2015. arXiv

[9] G. Dziuk and C. M. Elliott, *Finite elements on evolving surfaces*, IMA J. Numer. Anal. **27** (2007), no. 2, 262–292.

[10] G. Dziuk, D. Kröner, and T. Müller, *Scalar conservation laws on moving hypersurfaces*, Interfaces Free Bound. **15** (2013), no. 2, 203–236.

[11] M. Espedal, A. Fasano, and A. Mikelić, *Filtration in porous media and industrial application: lectures given at the 4th session of the Centro Internazionale Matematico Estivo*, Lect. Notes Math., no. 1734, Springer, Berlin, 2000.

[12] J. Giesselmann, *A convergence result for finite volume schemes on Riemannian manifolds*, M2AN Math. Model. Numer. Anal. **43** (2009), no. 5, 929–955.

[13] J. Giesselmann and P. G. LeFloch, *Formulation and convergence of the finite volume method for conservation laws on spacetimes with boundary*, preprint, 2016. arXiv

[14] A. Kurganov and D. Levy, *A third-order semidiscrete central scheme for conservation laws and convection-diffusion equations*, SIAM J. Sci. Comput. **22** (2000), no. 4, 1461–1488.

[15] _____ , *Central-upwind schemes for the Saint-Venant system*, M2AN Math. Model. Numer. Anal. **36** (2002), no. 3, 397–425.

[16] A. Kurganov, S. Noelle, and G. Petrova, *Semidiscrete central-upwind schemes for hyperbolic conservation laws and Hamilton–Jacobi equations*, SIAM J. Sci. Comput. **23** (2001), no. 3, 707–740.

[17] A. Kurganov and G. Petrova, *Central-upwind schemes on triangular grids for hyperbolic systems of conservation laws*, Numer. Methods Partial Differential Equations **21** (2005), no. 3, 536–552.

[18] _____ , *A second-order well-balanced positivity preserving central-upwind scheme for the Saint-Venant system*, Commun. Math. Sci. **5** (2007), no. 1, 133–160.

[19] A. Kurganov, G. Petrova, and B. Popov, *Adaptive semidiscrete central-upwind schemes for nonconvex hyperbolic conservation laws*, SIAM J. Sci. Comput. **29** (2007), no. 6, 2381–2401.

[20] A. Kurganov and E. Tadmor, *New high-resolution central schemes for nonlinear conservation laws and convection-diffusion equations*, J. Comput. Phys. **160** (2000), no. 1, 241–282.

[21] _____ , *New high-resolution semi-discrete central schemes for Hamilton–Jacobi equations*, J. Comput. Phys. **160** (2000), no. 2, 720–742.

[22] P. G. LeFloch, *Hyperbolic systems of conservation laws: the theory of classical and nonclassical shock waves*, Birkhäuser, Basel, 2002.

[23] _____ , *Hyperbolic conservation laws on spacetimes*, Nonlinear conservation laws and applications (A. Bressan, G.-Q. G. Chen, M. Lewicka, and D. Wang, eds.), IMA Vol. Math. Appl., no. 153, Springer, New York, 2011, pp. 379–391.

[24] _____ , *Structure-preserving shock-capturing methods: late-time asymptotics, curved geometry, small-scale dissipation, and nonconservative products*, Advances in numerical simulation in physics and engineering: lecture notes of the XV 'Jacques-Louis Lions' Spanish–French School (C. Parés, C. Vázquez, and F. Coquel, eds.), SEMA SIMAI, no. 3, Springer, Cham, 2014, pp. 179–222.

[25] P. G. LeFloch and H. Makhlof, *A geometry-preserving finite volume method for compressible fluids on Schwarzschild spacetime*, Commun. Comput. Phys. **15** (2014), no. 3, 827–852.

[26] P. G. LeFloch, H. Makhlof, and B. Okutmustur, *Relativistic Burgers equations on curved spacetimes: derivation and finite volume approximation*, SIAM J. Numer. Anal. **50** (2012), no. 4, 2136–2158.

[27] P. G. LeFloch and B. Okutmustur, *Hyperbolic conservation laws on spacetimes: a finite volume scheme based on differential forms*, Far East J. Math. Sci. **31** (2008), no. 1, 49–83.

[28] R. Lenormand, *Pattern growth and fluid displacements through porous media*, Physica A **140** (1986), no. 1–2, 114–123.

[29] R. Lenormand and C. Zarcone, *Role of roughness and edges during imbibition in square capillaries*, conference paper SPE-13264-MS, Society of Petroleum Engineers, 1984.

[30] R. J. LeVeque, *Finite volume methods for hyperbolic problems*, Cambridge University, 2002.

[31] J. D. Logan, *An introduction to nonlinear partial differential equations*, Wiley, New York, 1994.

[32] A. Meister and J. Struckmeier, *Central schemes and systems of balance laws*, Hyperbolic partial differential equations: theory, numerics and applications, Vieweg, Braunschweig, 2002, pp. 59–114.

[33] K. W. Morton and T. Sonar, *Finite volume methods for hyperbolic conservation laws*, Acta Numer. **16** (2007), 155–238.

[34] H. Nessyahu and E. Tadmor, *Nonoscillatory central differencing for hyperbolic conservation laws*, J. Comput. Phys. **87** (1990), no. 2, 408–463.

[35] J. A. Rossmanith, D. S. Bale, and R. J. LeVeque, *A wave propagation algorithm for hyperbolic systems on curved manifolds*, J. Comput. Phys. **199** (2004), no. 2, 631–662.

[36] C.-W. Shu and S. Osher, *Efficient implementation of essentially nonoscillatory shock-capturing schemes*, J. Comput. Phys. **77** (1988), no. 2, 439–471.

[37] N. Su, J. P. C. Watt, K. W. Vincent, M. E. Close, and R. Mao, *Analysis of turbulent flow patterns of soil water under field conditions using burgers equation and porous suction-cup samplers*, Aust. J. Soil Res. **42** (2004), no. 1, 9–16.

[38] M. E. Vázquez-Cendón, *Improved treatment of source terms in upwind schemes for the shallow water equations in channels with irregular geometry*, J. Comput. Phys. **148** (1999), no. 2, 497–526.

ABDELAZIZ BELJADID: beljadid@mit.edu
Department of Civil and Environmental Engineering, Massachusetts Institute of Technology, 77 Massachusetts Avenue, Cambridge, MA 02139, United States

PHILIPPE G. LEFLOCH: contact@philippelefloch.org
Laboratoire Jacques-Louis Lions & Centre National de la Recherche Scientifique, Université Pierre et Marie Curie (Paris 6), 4 Place Jussieu, 75258 Paris, France

Communications in Applied Mathematics and Computational Science

msp.org/camcos

Communications in Applied Mathematics
and Computational Science

vol. 12   no. 1   2017